# 阿根廷米纳毕戈塔斯地区 1：250 000 地球化学数据集

陈玉明　　陈秀法

(中国地质调查局发展研究中心，北京，100037)

**摘要：** 米纳毕戈塔斯地区（Mina Pirquitas）地处阿根廷西北部的安第斯山区，位于阿根廷西北部的新生代铜（金）及多金属成矿带内，是安第斯成矿带的组成部分。该区的岩性多样，火山岩、侵入岩发育，地质构造复杂，成矿地质条件优越，是阿根廷最主要的铜金等金属矿产资源的分布区。2010—2014 年中国地质调查局与阿根廷地质调查局合作开展 1：250 000 地球化学示范研究，在米纳比戈塔斯地区采集了 2470 件水系沉积物和土壤样品，采样粒级为−10 目～+60 目，平均采样密度 1.01 个/4 $km^2$。采用 X 射线荧光光谱法、等离子质谱法、原子荧光光谱法、发射光谱法、石墨炉原子吸收分光光度法和离子选择性电极法等分析了 39 种元素和氧化物，编制了单元素地球化学图和综合异常图，最终形成阿根廷北部米纳毕戈塔斯地区 1：250 000 地球化学集，包含有 2 470 件样品×39 种元素（氧化物）的原始分析数据表格一个，地球化学图集一套（含有 1 张地质图、一张采样点位图和 39 张元素（氧化物）地球化学图）。新发现单元素地球化学异常 487 处，综合异常 52 处，并圈出了具进一步工作价值的找矿远景区。这些数据和图件对该区的找矿、基础地质研究和环境工程等具有重要参考利用价值。

**关键词：** 阿根廷；米纳毕戈塔斯；地球化学；水系沉积物；数据集

**数据服务系统网址：** http://dcc.cgs.gov.cn

## 1 引言

2010 年 7 月 15 日，阿根廷联邦计划、投资和服务部与中国地质调查局签署了《地球化学填图项目合作协议》，双方合作在阿根廷西北部米纳毕戈塔斯地区开展 1：250 000 地球化学填图的示范研究。该项目 2010 和 2012 年被列为中国地质调查局的国外矿产资源风险勘查资金工作项目 (科合 10262A002 和科合 201210A06200202)。

米纳毕戈塔斯地区位于阿根廷西北部的安第斯山区 (图 1)，西侧以安第斯山脉为界与智利为邻，北部与玻利维亚接壤，包括 1：250 000 地质图幅 2366−I/2166−III 阿根廷

境内的范围，面积为 9 791 km$^2$。属干旱–半干旱高原区，年平均气温为 3 ℃ ~ 6 ℃。植被类型以高原灌木草甸为主。
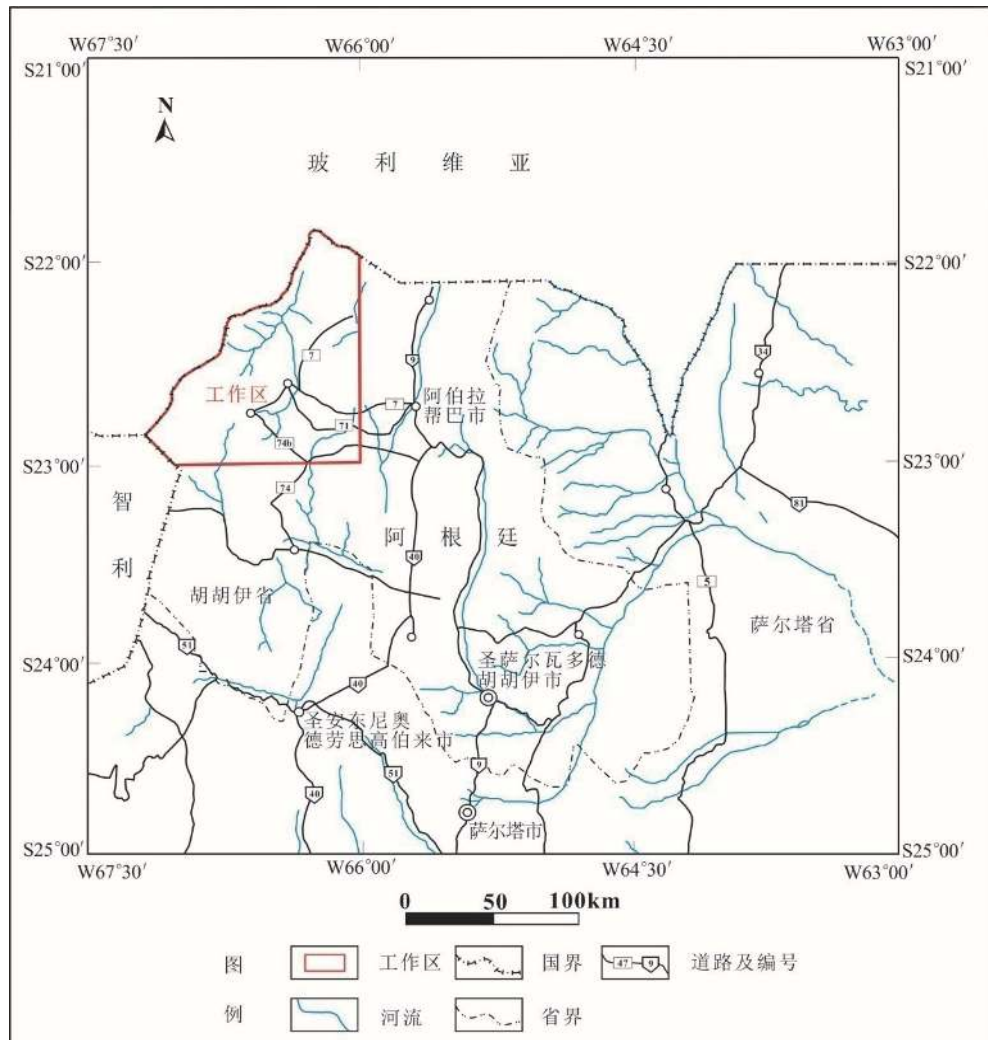


**图 1　阿根廷米纳毕戈塔斯工作区位置图**

工作区位于阿根廷西北部的新生代铜 (金) 及多金属成矿带内，属于安第斯成矿带的组成部分 (张潮等，2017d；陈念等，2017)。已探明的矿种主要包括铜、铅、锌、金、银、锂、锡、锑等 (陈玉明等，2013)。区内岩性多样，火山岩、侵入岩发育，地质构造复杂，成矿地质条件优越 (Bahiburg H. et al., 1991；张潮等，2017a；陈喜峰等，2017)，是阿根廷最主要的铜金矿分布区，主要矿床类型有斑岩型铜金 (钼) 矿、热液型金 (铜银) 矿、热液型锡和多金属矿，以及盐湖卤水型锂、钾、硼矿和砂金矿床 (Flexer Victoria et al., 2018；Rafaerl A. et al., 1999；Ricardo N. Alonso，1999a, b；张潮等，2017b；张潮等，2017c；崔敏利等，2017)。

本项目从 2010 年 7 月开始至 2014 年 6 月结束，历时 4 年，累计完成米纳毕戈塔斯地区 9 791 km$^2$ 1∶250 000 地球化学填图。最终成果为地球化学数据集，包括一个 Excel 表格，含有 2 470 件样品×39 种元素 (氧化物) 的原始分析数据 (表 1)；一个图集，含有 1 张地质图、1 张采样点位图和 39 张元素 (氧化物) 地球化学图。

<div align="center">表 1　数据库 (集) 元数据简表</div>

| 条　目 | 描　述 |
|---|---|
| 数据库(集)名称 | 阿根廷米纳毕戈塔斯地区1∶250 000地球化学数据集 |
| 数据库(集)作者 | 陈玉明，中国地质调查局发展研究中心<br>陈秀法，中国地质调查局发展研究中心 |
| 数据时间范围 | 2010年7月−2014年6月 |
| 地理区域 | 位于阿根廷共和国西北部，属阿根廷1∶25万图幅2366−I/2166−III范围，面积为9 791 km$^2$；中心坐标为：S 22°30′00″，W 66°30′00″ |
| 数据格式 | *.xlsx，*.jpg |
| 数据量 | 216MB |
| 数据服务系统网址 | http://dcc.cgs.gov.cn |
| 基金项目 | 中国地质调查局地质调查项目"海上丝绸之路重点地区有色金属资源潜力评价"（DD20160118），国外风险勘查资金工作项目"中阿合作阿根廷西北部地区1∶25万地球化学调查"（科合201210A06200202）和"阿根廷西北部地区铜（金）矿资源潜力调查与评价"（科合10262A002）联合资助 |
| 语种 | 中文、英文 |
| 数据库(集)组成 | 包括一个Excel表格， 含有2470件样品×39种元素(氧化物)的原始分析数据;一个图集，含有1张地质图、1张采样点位图和39张元素(氧化物)地球化学图 |

## 2　数据采集和处理方法

### 2.1　野外定点

　　采用高分辨率卫星图片和谷歌地球相结合的方式，生成 1∶50 000 地形影像图，并解译出水系和道路。这种方法成功地解决了没有 1∶50 000 地形图地区的地球化学采样底图问题。结合地形地物，GPS 定点误差不超过 15 m。

### 2.2　采样密度

　　设计采样密度为 1 个样品/4 km$^2$，在矿化区加密；在交通不便的边远地区采样密度适当降低。实际采样 2 470 个，平均采样密度 1.01 个/4 km$^2$。

### 2.3　采样方法

　　在水系发育区域，采集水系沉积物样品。采样点位选定在能够代表上游汇水域基岩成分、有利于多种粒级混杂沉积的现代河道的活动流水线上或河床底部。为提高每个样品的代表性，在采样点附近 30～50 m 范围内进行多点 (3～5 处) 采样，合并为一个组合样。羽状水系分布区，在采样单元内选择多条并列水系采样并组合成一个样品，样点标注在中间水系；遇到河道很宽时，以横切河道多点采样，并排除风成物干扰。通过实验确定的采样粒级为−10 目～+60 目，最终筛分出来的样品重量大于 300 g。

　　在水系不发育区域，采集土壤样品，采样部位为平原或山坡的残 (坡) 积物发育地段。样品介质主要为−10～+60 目的细粒碎屑物质，样品重量大于 300 g。为了增强样品的代表性，在采样点附近，在 50～100 m 范围内沿同一地形等高线多处采集单点样，组合成一个样品 (陈玉明等，2016)。

### 2.4　样品加工

　　样品加工基本流程为：自然干燥 (或低温烘干)→破碎→过筛→拌匀→缩分称重→填写标签→装袋→填写送样单、装箱入库。
　　①样品干燥方式采取日晒风干。干燥过程中及时揉搓样品，防止结块，并用木槌适

当敲击。

②用 10 目套 60 目不锈钢筛将样品充分过筛，截取重量大于 300 g 的样品。

③按四分法缩分出 150 g 作为分析样，用牛皮纸袋和塑料袋封装；150 g 作为副样，用牛皮纸袋封装。

④分析样运送至中国国土资源部长春矿产资源监督检测中心进行 39 种元素 (或氧化物) 分析，副样由阿根廷地质调查局长期保存。

## 3 数据样本描述

### 3.1 数据特征

阿根廷西北部米纳毕戈塔斯地区 1： 250 000 地球化学数据集，包括一个 Excel 表格—阿根廷西北部米纳毕戈塔斯地区 1： 250 000 地球化学分析数据，含有 2470 件样品的 Ag、As、Au、B、Ba、Be、Bi、Cd、Co、Cr、Cu、F、Hg、La、Li、Mo、Mn、Nb、Ni、P、Pb、Sb、Sn、Sr、Th、Ti、U、V、W、Y、Zr、Zn、$Al_2O_3$、CaO、MgO、$K_2O$、$Na_2O$、$SiO_2$、$Fe_2O_3$ 共 39 种元素 (氧化物) 的原始分析数据 (表 2)；还包括一个图集—阿根廷西北部米纳毕戈塔斯地区 1： 250 000 地球化学图集，含有 1 张地质图、一张采样点位图和 39 张元素 (氧化物) 地球化学图 (如图 2 所示)。

表 2 阿根廷米纳毕戈塔斯地区元素地球化学分析数据表[1]

| 序号 | 字符名称 | 数据类型 | 实例 | 序号 | 字符名称 | 数据类型 | 实例 |
|---|---|---|---|---|---|---|---|
| 1 | 分析批号 | 字符型 | a20128001-1 | 22 | Y | 浮点型 | 5000.74 |
| 2 | 实验室编号 | 字符型 | 1 | 23 | Zn | 浮点型 | 32.75 |
| 3 | 样品号 | 字符型 | HT23A301 | 24 | Zr | 浮点型 | 122.7 |
| 4 | As | 浮点型 | 20.3 | 25 | Li | 浮点型 | 201.9 |
| 5 | Sb | 浮点型 | 1.56 | 26 | Be | 浮点型 | 73.92 |
| 6 | Hg | 浮点型 | 0.01 | 27 | V | 浮点型 | 4.02 |
| 7 | Al | 浮点型 | 18.61 | 28 | Cr | 浮点型 | 130.85 |
| 8 | Ba | 浮点型 | 653 | 29 | Co | 浮点型 | 91.13 |
| 9 | CaO | 浮点型 | 0.15 | 30 | Ni | 浮点型 | 19.01 |
| 10 | Cu | 浮点型 | 25.6 | 31 | Mo | 浮点型 | 38.3 |
| 11 | $Fe_2O_3$ | 浮点型 | 5.85 | 32 | Cd | 浮点型 | 0.88 |
| 12 | $K_2O$ | 浮点型 | 4.29 | 33 | W | 浮点型 | 0.124 |
| 13 | La | 浮点型 | 47.5 | 34 | Bi | 浮点型 | 2.55 |
| 14 | MgO | 浮点型 | 1.37 | 35 | Th | 浮点型 | 0.59 |
| 15 | Mn | 浮点型 | 593.74 | 36 | U | 浮点型 | 17.12 |
| 16 | $Na_2O$ | 浮点型 | 0.7 | 37 | B | 浮点型 | 3.53 |
| 17 | Nb | 浮点型 | 18.68 | 38 | Sn | 浮点型 | 68.8 |
| 18 | P | 浮点型 | 460.85 | 39 | Ag | 浮点型 | 5.3 |
| 19 | $SiO_2$ | 浮点型 | 25.7 | 40 | F | 浮点型 | 704.7 |
| 20 | Sr | 浮点型 | 63.06 | 41 | Au | 浮点型 | 0.71 |
| 21 | Ti | 浮点型 | 52.2 | | | | |

注1：元素含量单位：Au，$\times 10^{-9}$；$Fe_2O_3$、$Al_2O_3$、CaO、MgO、$Na_2O$、$K_2O$、$SiO_2$，$\times 10^{-2}$；其他元素$\times 10^{-6}$

阿根廷西北部米纳毕戈塔斯地区铜地球化学图

The copper geochemical map of the Mina Pirquitas region of the northwest Argentina
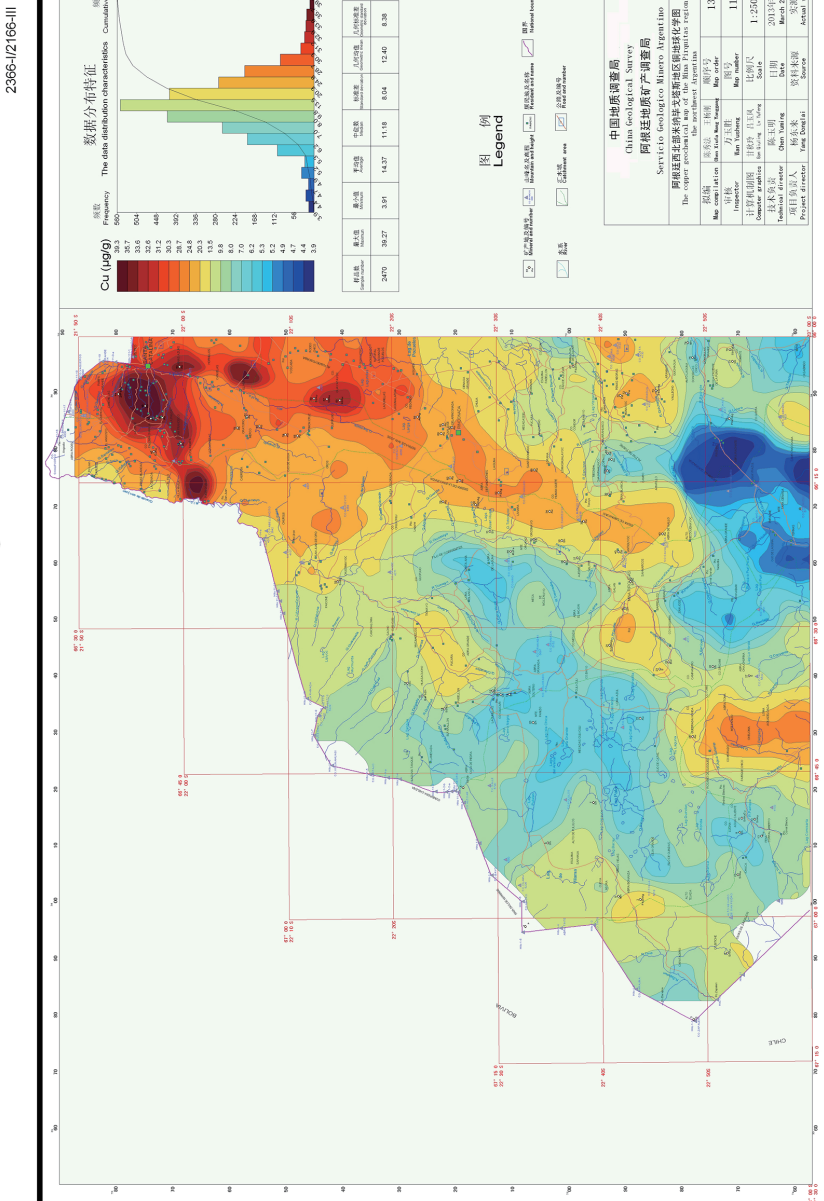
图 2　阿根廷米纳毕戈塔斯地区铜元素地球化学图

### 3.2 地质特征和分区

本区出露的最古老地质体是奥陶纪的砂岩、花岗岩和花岗斑岩 (Voldman G. et al., 2018)。侏罗纪发生了广泛的构造运动和区域变质作用，导致地层褶皱并轻微变质。白垩纪局部接受沉积，古近纪和新近纪以大规模的造山运动和火山喷发沉积为特征 (Bahiburg H. et al., 1991；张潮等，2017a；陈玉明等，2017)。为了解元素在不同地质体中的分布规律，根据岩性差异，项目组将全区划分为 7 个地质子区 (图 3)：
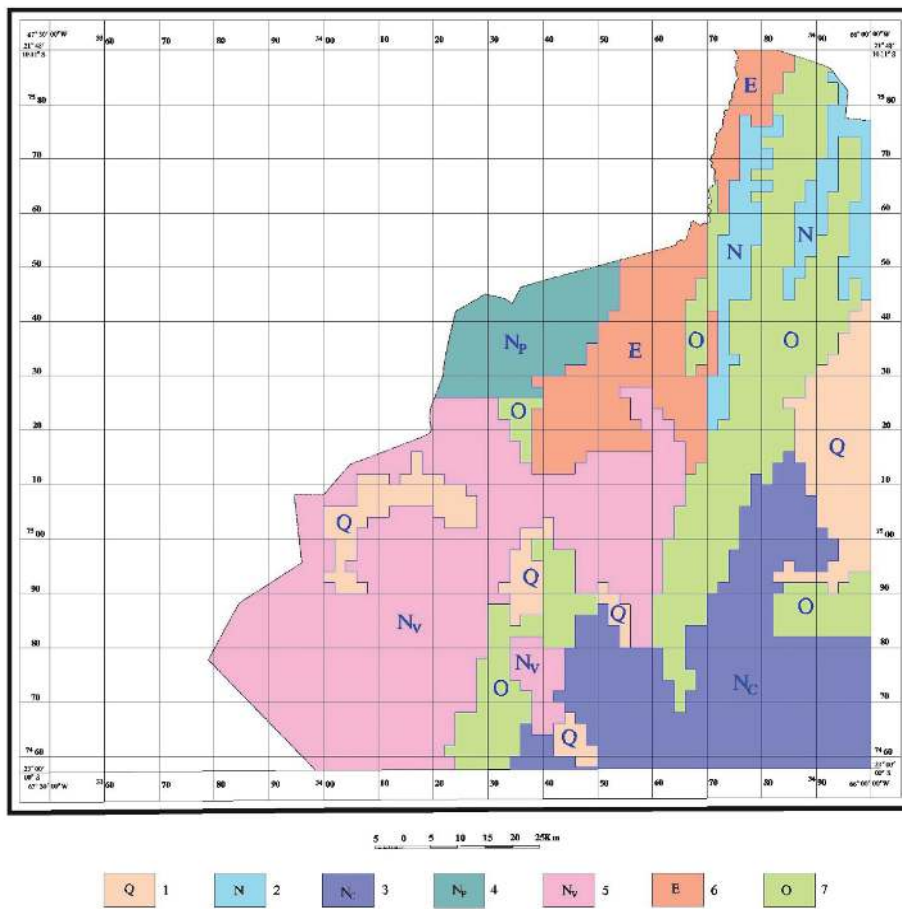


**图 3 阿根廷米纳毕戈塔斯地区地质子区分区图**

1-第四系冲积层；2-新近系沉积岩；3-新近系 CORANZULI 火山杂岩；4-新近系 PANIZOS 火山杂岩；
5-新近系 VTLAMA 火山杂岩；6-古近系沉积岩；7-奥陶系沉积岩

(1) 第四系冲积层子区 (Q)；

(2) 新近系沉积岩子区 (N)；

(3) 新近系 CORANZULI 火山杂岩子区 (Nc)；

(4) 新近系 PANIZOS 火山杂岩子区 (Np)；

(5) 新近系 VTLAMA 火山杂岩子区 (Nv)；

(6) 古近系沉积岩子区 (E)；

(7) 奥陶系沉积岩子区 (O)。

### 3.3 元素地球化学特征

统计每个地质子区水系沉积物的元素含量发现，所有元素及氧化物在全域范围内都

不符合正态分布，说明样本是来自多重母体或该区经历了至少两次以上地质作用或地球化学作用，地质背景差异较大，从而使元素的含量分布不均匀，造成其概率分布复杂化。

  本次研究统计了全域及各子区的元素平均含量，用以反映本区元素在不同地质子区中的含量变化特征 (表 3)。

表 3    阿根廷米纳毕戈塔斯地区各地质子区元素参数特征对比表

| 地质子区 | Q | N | Nc | Np | Nv | E | O |
|---|---|---|---|---|---|---|---|
| 高于全域平均值1.2倍的元素或氧化物 | W、Cd | Au、As、Sb、Bi、Mo、B、Co、Cr、Cu、La、Ni、V、Y、Zn | Be、Sr、$Fe_2O_3$、$Na_2O$、CaO | F、Ti、Ba、Mn、Nb、P、CaO、MgO | Sr、V、$Fe_2O_3$、$Na_2O$、CaO | Ag、CaO | Au、Sb、Bi、Cd、B、Co、Cr、Cu、Ni、V、Y、Zn、$Fe_2O_3$ |
| 高于全域平均值及对数方差的元素或氧化物 | Ag、Hg、Cd | Au、Ba、La、Nb | W、Be、Pb、$SiO_2$ | Mn | Sn | Cd | Au、Sb、Cu |

  从表 3 可以看出，水系沉积物中元素含量明显高于全区背景含量的元素组合，在新近系沉积岩子区 (N) 与奥陶系沉积岩子区 (O) 较为相似，以贵金属 Au、有色金属 As、Sb、Bi、Mo、Cu、Zn，以及亲铁元素 Co、Cr、Ni、V 和 $Fe_2O_3$ 等元素为主，而三个新近系火山杂岩子区 (Nc、Np、Nv) 都具有 Be、Sr、$Fe_2O_3$、$Na_2O$、CaO、MgO、Ti、V 等高含量的元素及氧化物组合。第四系冲积层子区 (Q) 中 W、Cd 富集，古近系沉积岩子区 (E) Ag、CaO 富集，水系沉积物中这些元素和氧化物的高含量反映了所在区域内原岩的元素地球化学含量分布特点。

  在奥陶系沉积岩子区 (O) 内，水系沉积物中 Au、Sb、Cu 的含量高，离散度大，表明该区为 Au、Sb、Cu 成矿的重要地区。实际上，本区脉状金、锑−金矿床和少量热液角砾岩型锑−金矿就蕴含在奥陶系沉积岩中。

## 4    数据质量控制和评估

  39 种元素 (氧化物) 分析测试由中国国土资源部长春矿产资源监督检测中心承担。分析元素和氧化物为：B、Cd、As、Hg、Sb、Mo、F、Co、Cr、Cu、Mn、Ni、P、Pb、Zn、$SiO_2$、$Al_2O_3$、$Fe_2O_3$、$K_2O$、$Na_2O$、CaO、MgO、Ag、W、Sn、Bi、Au、Be、La、Nb、Li、Y、Zr、U、Th、V、Ti、Sr、Ba。分析方法以 X 射线荧光光谱法 (XRF) 为主，辅以 ICP-Ms(等离子质谱法)、AFS(原子荧光光谱法)、AES(发射光谱法)、GFAAS(石墨炉原子吸收分光光度法) 和 ISE(离子选择性电极法)。每一种元素 (氧化物) 的分析方法、分析方法的检出限、区域地球化学勘查规范 (DZ/T0167−2006) 要求的检出限、以及报出率等列于表 4。

表 4    分析方法的检出限以及分析元素报出率

| 元素编号 | 被检测的元素 | | 分析方法的检出限 | 规范要求的检出限 | 报出率(%) | 分析方法 |
|---|---|---|---|---|---|---|
| 1 | As | 砷 | 1 | 1 | 99.90 | AFS |
| 2 | B | 硼 | 2 | 5 | 98.42 | AES |
| 3 | Sb | 锑 | 0.05 | 0.1 | 100.0 | AFS |
| 4 | Cd | 镉 | 0.05 | 0.05 | 98.69 | ICP−Ms |
| 5 | Au | 金 | 0.3 | 0.3 | 99.95 | GFAAS |

续表 4

| 元素编号 | 被检测的元素 | | 分析方法的检出限 | 规范要求的检出限 | 报出率(%) | 分析方法 |
|---|---|---|---|---|---|---|
| 6 | Co | 钴 | 0.6 | 1 | 100.0 | ICP-Ms |
| 7 | Cr | 铬 | 5 | 15 | 100.0 | ICP-Ms |
| 8 | Cu | 铜 | 1 | 1 | 100.0 | XRF |
| 9 | F | 氟 | 100 | 100 | 100.0 | ISE |
| 10 | Hg | 汞 | 0.000 5 | 0.000 5 | 100.0 | AFS |
| 11 | Li | 锂 | 1 | 5 | 100.0 | ICP-Ms |
| 12 | Mn | 锰 | 13 | 30 | 100.0 | XRF |
| 13 | Mo | 钼 | 0.3 | 0.4 | 97.92 | ICP-Ms |
| 14 | Be | 铍 | 0.4 | 0.5 | 100.0 | ICP-Ms |
| 15 | Ni | 镍 | 1.2 | 2 | 100.0 | ICP-Ms |
| 16 | P | 磷 | 19 | 100 | 100.0 | XRF |
| 17 | Pb | 铅 | 2 | 2 | 100.0 | XRF |
| 18 | U | 铀 | 0.3 | 0.5 | 100.0 | ICP-Ms |
| 19 | W | 钨 | 0.3 | 0.5 | 99.97 | ICP-Ms |
| 20 | Zn | 锌 | 3 | 10 | 100.0 | XRF |
| 21 | Th | 钍 | 1 | 4 | 100.0 | ICP-Ms |
| 22 | Bi | 铋 | 0.06 | 0.1 | 100.0 | ICP-Ms |
| 23 | $Al_2O_3$ | 三氧化二铝 | 0.03 | 0.05 | 100.0 | XRF |
| 24 | $SiO_2$ | 二氧化硅 | 0.06 | 0.1 | 100.0 | XRF |
| 25 | $Fe_2O_3$ | 三氧化二铁 | 0.04 | 0.05 | 100.0 | XRF |
| 26 | CaO | 氧化钙 | 0.02 | 0.05 | 100.0 | XRF |
| 27 | MgO | 氧化镁 | 0.04 | 0.05 | 100.0 | XRF |
| 28 | $K_2O$ | 氧化钾 | 0.02 | 0.05 | 100.0 | XRF |
| 29 | $Na_2O$ | 氧化钠 | 0.03 | 0.05 | 100.0 | XRF |
| 30 | Nb | 铌 | 1 | 5 | 100.0 | XRF |
| 31 | Sr | 锶 | 3 | 5 | 100.0 | XRF |
| 32 | Ti | 钛 | 30 | 100 | 100.0 | XRF |
| 33 | V | 钒 | 4 | 20 | 100.0 | ICP-Ms |
| 34 | Y | 钇 | 1 | 5 | 100.0 | XRF |
| 35 | Zr | 锆 | 2 | 10 | 100.0 | XRF |
| 36 | Ba | 钡 | 13 | 50 | 100.0 | XRF |
| 37 | La | 镧 | 8 | 30 | 100.0 | XRF |
| | La | 镧 | 1 | 30 | 100.0 | ICP-Ms |
| 38 | Sn | 锡 | 0.8 | 1 | 100.0 | AES |
| 39 | Ag | 银 | 0.02 | 0.02 | 99.97 | AES |
| 合计 | | | | | 99.86 | |

注：XRF，X射线荧光光谱法；ICP-Ms，等离子质谱法；AFS，原子荧光光谱法；AES，发射光谱法；GFAAS，石墨炉原子吸收分光光度法；ISE，离子选择性电极法。

质量管理采用外部质量监控和内部质量监控相结合、以外部质量监控为主的原则，外部质量监控是按 8% 的比例插入标准控制样，共插入 208 件。内部质量监控是每

50 件分析样品为一组，插入 4 个水系沉积物一级标准物质 (GSD2a、GSD8a、GSD22、GSD4a)，计算单次测定值与标准值之间的对数差以控制分析的准确度；计算 4 个监控样对数差的标准偏差，用以衡量同批样品的精密度。

金的分析质量监控：每 50 件样品中密码插入 4 个标准物质 (GAu2b、GAu7b、GAu10b、GAu11b 对应含量分别为 0.9、3.1、5.1、10.5) 作为金分析监控样。

内检样品及异常点质量监控：内检样品按样品总数的 5% 进行检查分析。对部分元素含量较高或较低的样品进行异常值抽查。各元素 (或项目) 的内检分析和异常值抽查的质量控制均按相对偏差 |$RD\%$|≤25% 统计合格率。

本次所有监控样的 39 种元素的合格率为 100%。

按所送样品总数随机抽取 5% 作为内检样品，内检总数为 132 件，内检总项数为 5 148 项，内检总体合格率为 99.51%。

为了避免由于分析偶然误差而造成的地球化学假象，在每批样品分析完毕后，都对部分分析结果的突变高点和低点进行重复性检验。异常点抽查的总项数为 1 153 项，总合格项数 1 142 项，总合格率为 99.04%。内检样品与异常值抽查的总体合格率 99.42%。

## 5　数据处理

本次数据处理与制图采用了中国地质调查局发展研究中心开发的 Geoexpl 2012 数据处理软件。数据处理方法如下：

(1) 数据网格化

网格距为 4 km×4 km，搜索半径为 10 km，采用指数加权法。

(2) 元素地球化学图

以 4 km$^2$ 的网格数据用计算机直接绘制等量线图。采用累积频率分级方法确定等量线的间隔。色区的划分使用累积频率法成图，色区划分为：<1.5% 深蓝色、1.5%～15% 蓝色、15%～25% 浅蓝色、25%～75% 浅黄色、75%～85% 浅红色、95%～98.5% 深红色、>98.5% 深红色。

(3) 质量保证

编图及资料整理中全部原始数据的转录、上图及计算都进行 100% 复核。

## 6　结论

中国地质调查局与阿根廷地质调查局合作开展阿根廷米纳毕戈塔斯地区 1：250 000 水系沉积物地球化学填图工作，历时 4 年，获得了珍贵的第一手境外地球化学测量数据资料，包括 2 470 件水系沉积物和土壤样品的 39 种元素和氧化物的原始分析数据，以及以此为基础形成的系列地球化学图。新发现单元素地球化学异常 487 处，综合异常 52 处，并圈出了具进一步工作价值的远景区 2 处。进一步研究并挖掘这些数据和图件的信息，对该区的找矿、基础地质研究和环境工程等具有重要参考利用价值。

## 参考文献

Bahiburg H., Breitkreuz C 1991. Paleozoic Evolution of Active Margin Basins in the Southern Central Andes (Northweatern Argentina and Northern Chile)[J]. Journal of South American Earth Sciences, 4(3): 171−188.

Flexer Victoria, Fernando Baspineiro Celso, Ines Galli, Claudia. 2018. Lithium Recovery from Brines: A Vital Raw Material for Green Energies with a Potential Environmental Impact in Its Mining and Processing[J]. Science of the Total Environment, 639: 1188−1204.

Rafaerl A. A. 1999. Depositos de Sulfato de Sodio de Jujuy, Salta y Catamarca [M], Eduardo O. Zappettini, Recursos Minerale de la Republica Argentian, Publicado con la Colaboracion de la Fundacion Empremin, Buenos Aires, Instituto de Geologia y Minerales-SEGEMAR, 1922−1925.

Ricardo N. Alonso, 1999a. Boratos terciarios de la Puna, Jujuy, Salta y Catamarca [M], Eduardo O. Zappettini, Recursos Minerale de la Republica Argentian, Publicado con la colaboracion de la Fundacion Empremin, Buenos Aires, Instituto de Geologia y Minerales-SEGEMAR: 1779−1826.

Ricardo N. Alonso. 1999b. Los Salares de la Puna y sus Recursos Evaporiticos, Jujuy, Salta y Catamarca [A], Eduardo O. Zappettini, Recursos Minerale de la Republica Argentian [C], Publicado con la colaboracion de la Fundacion Empremin, Buenos Aires, Instituto de Geologia y Minerales-SEGEMAR: 1905−1921.

Voldman Gustavo G., Alonso Juan L., Fernandez Luis P 2018. Cambrian-Ordovician Conodonts from Slump Deposits of the Argentine Precordillera: New Insights into Its Passive Margin Development[J]. Geological Magazine, 155(1): 85−97.

陈念, 毛景文, 范成龙, 陈玉明. 2017. 秘鲁 Don Javier 斑岩型铜钼矿床矿化蚀变特征及矿床三维勘查模型[J]. 矿床地质, 36(3): 705−718.

陈喜峰. 2017. 南美洲铝土矿资源勘查开发现状与潜力分析[J]. 国土资源科技管理, 34(1): 106−115.

陈玉明, 邓小林. 2013. 阿根廷锂资源潜力及开发利用现状[J]. 盐湖研究 (4): 67−72.

陈玉明, 夏修展, 甘秋铃, 耿林, 杨刚. 2016. 阿根廷米纳毕戈塔地区水系沉积物采样粒度试验研究[J]. 地质找矿论丛, 31(2): 295−302.

陈玉明, 张 潮, 陈秀法等. 2017. 南美洲地质矿产与矿业开发 (M). 武汉: 中国地质大学出版社.

崔敏利, 张作伦, 陈玉明, 陈方戈. 2017. 南美洲大型-超大型金矿地质特征与成矿作用研究[J]. 中国地质, 44(4): 642−663.

张潮, 陈玉明, 赵宏军. 2017a. 南美洲成矿区带划分[J]. 地质通报, 36(12): 2134−2142.

张潮, 陈玉明, 陈喜峰. 2017b. 阿根廷金矿床时空分布规律[J]. 地质通报, 36(12): 2154−2163.

张潮, 陈玉明, 赵宏军, 元春华. 2017c. 南美洲铜矿时空分布规律[J]. 地质论评, 63(Supp.): 29−30.

张潮, 陈玉明, 赵宏军. 2017d. 南美洲中安第斯地区构造-岩浆事件与成矿[J]. 地质论评, 63(Supp.): 17−18.

# Argentine Mina Pirquitas 1：250 000 Geochemistry Dataset

CHEN Yuming, CHEN Xiufa

(*Development and Research Center of China Geological Survey*, *Beijing* 100037, *China*)

**Abstract:** Mina Pirquitas, situated in the Andes Mountain of northwest Argentina, and within the Cenozoic Cu (Au) and polymetal metallogenic belt, is a part of Andes metallogenic belt. The region is diverse in lithology, well developed in volcanic and intrusive rocks, complex in geological structure, advantageous in metallogenic geological conditions, and thus the most prominent distribution region of metallic mineral resources such as Au and Cu in Argentina. From 2010 to 2014, China Geological Survey (CGS) and Argentina Geological Survey (AGS) cooperated on 1：250 000 geochemistry research demonstration during which 2 470 fluvial sediment and soil samples were collected in Mina Pirquitas at a sample grain−size ranging between -10 meshes and +60 meshes and at a mean sampling density of 1.01 samples/4 km$^2$. 39 elements and oxides were analyzed with X−ray fluorescence spectroscopy, plasma−mass spectrometry, atomic fluorescence spectrometry, atomic emission spectrometry, graphite furnace atomic absorption spectrometry and ion selective electrode method, and single−element geochemical maps and comprehensive anomaly maps were plotted. A total of 487 locations with single−element geochemistry anomaly and 52 locations with comprehensive anomaly were discovered and prospective mineral areas worthy of further investigation were delineated. These data and maps are important for reference to mineral exploration, fundamental geological research, and environmental engineering in the region.
**Key words:** Argentina; Mina Pirquitas; Geochemistry; Fluvial sediment; Dataset
**Data service system URL:** http://dcc.cgs.gov.cn

## 1　Introduction

On July 15, 2010, Argentine Federal Ministry of Planning, Ministry of Investment and Service signed the *Cooperation Agreement on Geochemical map Plotting Projects* with CGS to jointly conduct a research demonstration for 1：250 000 geochemical map plotting in Mina Pirquitas of northwest Argentina. In 2010 and 2012, this project was recognized as one of the work projects of CGS under foreign venture exploration fund (Kehe 10262A002 and Kehe

201210A06200202).

　　Mina Pirquitas is located in the Andes Mountain Region in northwest Argentina (Fig. 1), bounded by the Andes Mountains of Chile in the west and bordering Bolivia in the north, and covers the range of 2366-I/2166-III Argentine portion of the 1∶250 000 geologic map sheet, with an area of 9 791 km$^2$. It is an arid to semi−arid plateau, with an annual mean temperature of 3°C~6°C. Vegetation is dominantly plateau shrub meadow.
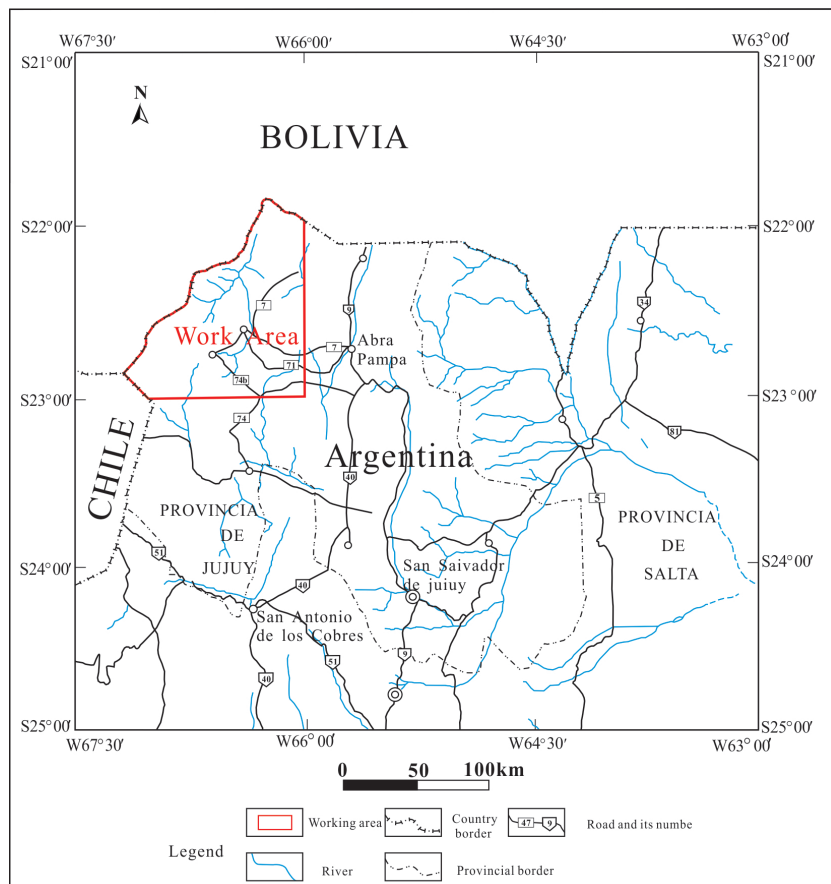


**Fig. 1　Map showing the working area location in Mina Pirquitas, Argentina**

　　The working area, located in the the Cenozoic Cu (Au) and polymetal metallogenic belt in northwest Argentina, is a part of Andes metallogenic belt (Zhang C et al., 2017d; Chen N et al., 2017). Proven mineral species predominantly include Cu, Pb, Zn, Au, Ag, Li, Sn and Sb etc. (Chen YM et al., 2013). The region is diverse in lithology, well developed in volcanic and intrusive rocks, complex in geological structure, and advantageous in metallogenic geological conditions (Bahiburg H. et al., 1991; Zhang C et al., 2017a; Chen XF et al., 2017). Consequently, it is one of the most prominent distribution region of metallic mineral resources such as Au and Cu in Argentina, with main deposit types including porphyry-type Cu−Au (Mo) deposit, hydrothermal Au (Cu−Ag) deposit, hydrothermal Sn and polymetal deposit, as well as salt lake−brine Li, K, B deposits and gold placer (Flexer Victoria et al., 2018; Rafaerl A. et al., 1999; Ricardo N. Alonso, 1999a, b; Zhang C et al., 2017b; Zhang C et al., 2017c; Cui ML et al., 2017).

　　The project has been done for four years beginning in July 2010 and ending in June 2014,

having completed 1：250 000 geochemical map plotting of 9,791 $km^2$ in Mina Pirquitas. The ultimate achievement is a geochemistry dataset, including an Excel sheet containing raw analytical data of 2,470 samples × 39 elements (oxides) (Table 1) and an atlas containing a geologic map, a sampling location map and 39 element (oxide) geochemical maps.

**Table 1    Simplified metadata table of the database (dataset)**

| Items | Description |
| --- | --- |
| Database (dataset) name | Argentine Mina Pirquitas 1：250 000 Geochemistry Dataset |
| Database (dataset) authors | Chen Yuming, Development and Research Center of China Geological Survey <br> Chen Xiufa, Development and Research Center of China Geological Survey |
| Data acquisition time | July 2010—June 2014 |
| Geographic area | In the northwest of the Republic of Argentina, within the range of 2366-I/2166-III in Argentine 1：250 000 map sheet, with an area of 9,791 $km^2$; left coordinates: S 22°30′00″, W 66°30′00″ |
| Data format | .xlsx, .jpg |
| Data size | The Excel datasheet containing analytical data of 2 470 samples and 39 elements (oxides) is 663 KB and the atlas containing 41 maps is 215MB |
| Data service system URL | http://dcc.cgs.gov.cn |
| Fund project | Jointly funded by CGS geological survey project "Elevation of Nonferrous-metal Resource Potential in Prioritized Region Along Maritime Silk Road"(DD20160118), the project "Northwest Argentine 1:250 000 Geochemistry Survey under Sino-Argentine Cooperation" (Kehe 201210A06200202) under foreign venture exploration fund and "Survey and Elevation of Cu (Au) Mineral Resource Potential in Northwest Argentina" (Kehe 10262A002) |
| Language | Chinese, English |
| Database (dataset) composite | The database (dataset) consists of an Excel sheet and an atlas: Northwest Argentine Mina Pirquitas 1:250 000 Geochemistry Dataset and Northwest Argentine Mina Pirquitas 1:250 000 Geochemistry Atlas |

## 2    Data Acquisition and Processing

### 2.1    Point Fixation in the Field

High-resolution satellite images and Google Earth were combined to generate 1：50 000 topographical image maps, interpreting drainage systems and roads at the same time. This method succeeded in solving the problem of base maps for geochemistry sampling at places where there is no 1：50 000 topographical map. Combined with topography and surface features, the error in point fixation with GPS is less than 15 m.

### 2.2    Sampling Density

The designed sampling density is 1 sample/4 $km^2$, which is increased in any mineralization area and lowered properly in remote areas where traffic is inconvenient. A total of 2,470 samples were taken, with a mean sampling density of 1.01 sample/4 $km^2$.

### 2.3    Sampling Methods

In areas with developed drainage systems, fluvial sediment samples were taken.Sampling points were selected at active water−flow lines or riverbed bottom of modern watercourses capable of representing bedrock components of upstream catchment and in favor of hybrid

sedimentation of particles of multiple sizes. To make each sample more representative, samples were taken at multiple points (3~5) within 30~50 m around the fixed sampling point, to be combined into a composite sample. In areas distributed with pinnate drainage systems, samples were taken from selected multiple parallel drainage systems and then combined into one sample. The sampling point was marked on the mid−drainage system, and in the case of a wider watercourse, samples were taken at multiple points traversing the watercourse and were eliminated when interference with aeolian material. The particle sizes were determined to be −10 meshes ~ +60 meshes by experiments, and final sample weight from the screen was more than 300 g.

In areas without developed drainage systems, soil samples were taken at eluvium (slope−wash) developed sites of plains or slopes. Sample medium was fine−grained detrital materials with a main grain size from −10 to +60 meshes and a sample weight of more than 300g. To make samples more representative, samples were taken at multiple points along the same contour line of the same topography within 50~100 m around the sample point to be combined into a sample (Chen YM et al., 2016).

### 2.4　Sample Processing

The basic procedure to process samples: naturally drying (or low−temperature drying) → crushing → sieving →mixing thoroughly → splitting and weighing → filling the label → putting samples into bags → filling the sample delivery order and putting sample bag into boxes for storage.

① Sample drying method: dry the sample under sunlight and air. During drying, rub and knead samples timely to prevent caking, and use a mallet to strike them properly.

② Use a 10−mesh plus 60−mesh stainless steel sieve to screen fully samples to get samples weighing over 300 g.

③ Using inquartation, split 150 g as an analytical sample packed in kraft paper bags and plastic bags; use the remaining 150 g as a duplicate sample, also packed in kraft paper bags.

④ Send the analytical samples to Changchun Mineral Resource Supervision and Testing Center, Ministry of Natural Resources (MNR), China to analyze 39 elements (or oxides) while duplicate samples were sent to AGS for long−term preservation..

## 3　Description of Data Samples

### 3.1　Data Features

Northwest Argentine Mina Pirquitas 1：250 000 Geochemistry Dataset consists of an Excel sheet (Northwest Argentine Mina Pirquitas 1：250 000 Geochemistry Data), which includes raw analytical data on 39 elements (oxides), i.e. Ag, As, Au, B, Ba, Be, Bi, Cd, Co, Cr, Cu, F, Hg, La, Li, Mo, Mn, Nb, Ni, P, Pb, Sb, Sn, Sr, Th, Ti, U, V, W, Y, Zr, Zn, $Al_2O_3$, CaO, MgO, $K_2O$, $Na_2O$, $SiO_2$ and $Fe_2O_3$ from 2,470 samples (Table 2); and an atlas (Northwest Argentine Mina Pirquitas 1：250 000 Geochemistry Atlas), which includes 1 geologic map, 1 sampling location map and 39 element (oxide) geochemical maps (as shown in Fig. 2).

**Table 2    Argentine Mina Pirquitas element geochemistry analytical datasheet[1]**

| No. | Character name | Data category | Example | No. | Character name | Data category | Example |
|---|---|---|---|---|---|---|---|
| 1 | Analysis lot No. | Character type | a20128001-1 | 22 | Y | Floating-point type | 5000.74 |
| 2 | Lab No. | Character type | 1 | 23 | Zn | Floating-point type | 32.75 |
| 3 | Sample No. | Character type | HT23A301 | 24 | Zr | Floating-point type | 122.7 |
| 4 | As | Floating-point type | 20.3 | 25 | Li | Floating-point type | 201.9 |
| 5 | Sb | Floating-point type | 1.56 | 26 | Be | Floating-point type | 73.92 |
| 6 | Hg | Floating-point type | 0.01 | 27 | V | Floating-point type | 4.02 |
| 7 | Al | Floating-point type | 18.61 | 28 | Cr | Floating-point type | 130.85 |
| 8 | Ba | Floating-point type | 653 | 29 | Co | Floating-point type | 91.13 |
| 9 | CaO | Floating-point type | 0.15 | 30 | Ni | Floating-point type | 19.01 |
| 10 | Cu | Floating-point type | 25.6 | 31 | Mo | Floating-point type | 38.3 |
| 11 | $Fe_2O_3$ | Floating-point type | 5.85 | 32 | Cd | Floating-point type | 0.88 |
| 12 | $K_2O$ | Floating-point type | 4.29 | 33 | W | Floating-point type | 0.124 |
| 13 | La | Floating-point type | 47.5 | 34 | Bi | Floating-point type | 2.55 |
| 14 | MgO | Floating-point type | 1.37 | 35 | Th | Floating-point type | 0.59 |
| 15 | Mn | Floating-point type | 593.74 | 36 | U | Floating-point type | 17.12 |
| 16 | $Na_2O$ | Floating-point type | 0.7 | 37 | B | Floating-point type | 3.53 |
| 17 | Nb | Floating-point type | 18.68 | 38 | Sn | Floating-point type | 68.8 |
| 18 | P | Floating-point type | 460.85 | 39 | Ag | Floating-point type | 5.3 |
| 19 | $SiO_2$ | Floating-point type | 25.7 | 40 | F | Floating-point type | 704.7 |
| 20 | Sr | Floating-point type | 63.06 | 41 | Au | Floating-point type | 0.71 |
| 21 | Ti | Floating-point type | 52.2 | | | | |

Note 1: Unit for element content: Au: $\times 10^{-9}$; $Fe_2O_3$, $Al_2O_3$, CaO, MgO, $Na_2O$, $K_2O$, $SiO_2$: $\times 10^{-2}$; other elements; $\times 10^{-6}$

### 3.2    Geological Characteristics and Zoning

In the region, the oldest outcropped geological body is Ordovician sandstone, granite and granite porphyry (Voldman G. et al., 2018). Widespread tectonic movement and regional metamorphism occurred during Jurassic, resulting in folded and slightly metamorphosed strata. And sedimentation occurred locally during Cretaceous, while large scale orogenesis and volcanic eruption-sedimentation developed during Paleogene and Neogene (Bahiburg H. et al., 1991; Zhang C et al., 2017[a]; Chen YM et al., 2017). To understand how elements are regularly distributed in different geological bodies, the whole region was divided into 7 geological sub−regions by lithology (Fig. 3 and Table 3):

(1) Quaternary alluvium sub−region (Q);

(2) Neogene sedimentary rock sub−region (N);

(3) Neogene CORANZULI volcanic complex sub−region (Nc);

(4) Neogene PANIZOS volcanic complex sub−region (Np);

(5) Neogene VTLAMA volcanic complex sub−region (Nv);

(6) Paleogene sedimentary rock sub−region (E);

(7) Ordovician sedimentary rock sub−region (O).

阿根廷西北部米纳毕戈塔斯地区铜地球化学图

The copper geochemical map of the Mina Pirquitas region of the northwest Argentina
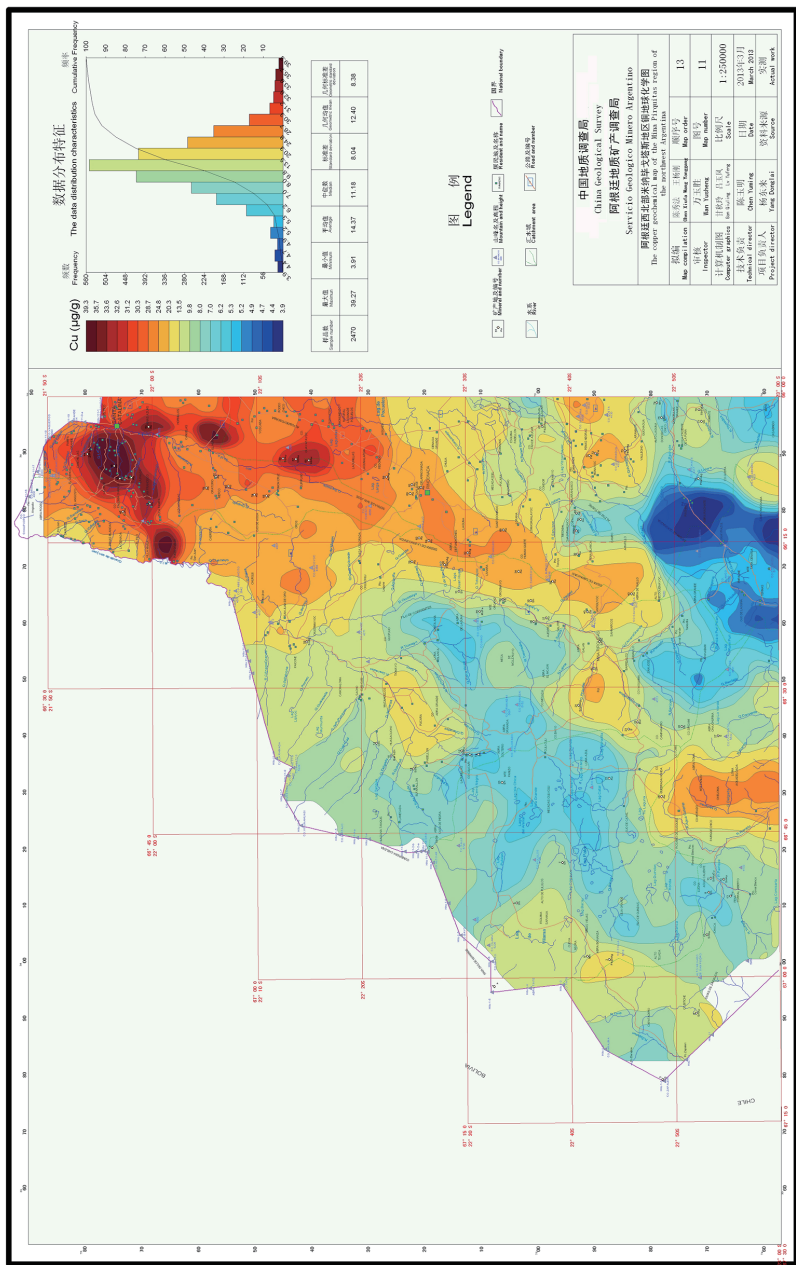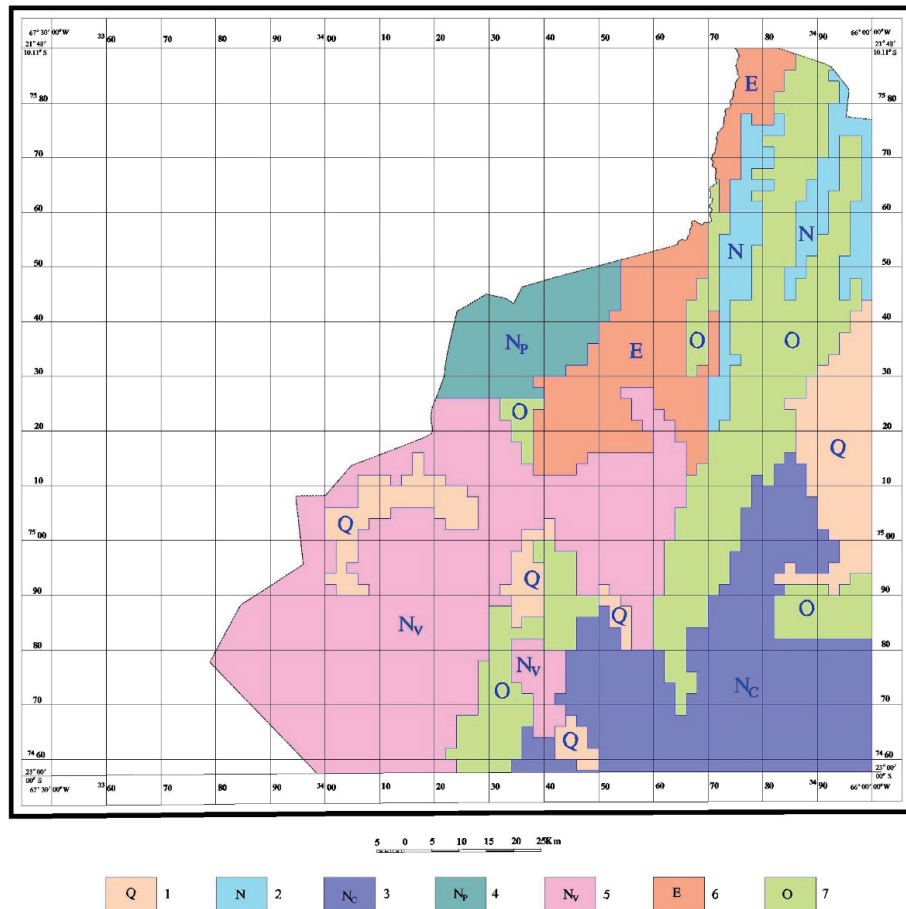
**Fig. 2   Cu geochemical map of the Mina Pirquitas Region of northwest Argentina**

**Fig. 3    Geological sub-region map**

1−Quaternary alluvium; 2−Neogene sedimentary rock; 3−Neogene CORANZULI volcanic complex;
4−Neogene PANIZOS volcanic complex; 5−Neogene VTLAMA volcanic complex; 6−Paleogene sedimentary rock;
7−Ordovician sedimentary rock

**Table 3    Characteristic comparison in element parameters of geological sub-regions**

| Geological sub-regions | Q | N | Nc | Np | Nv | E | O |
|---|---|---|---|---|---|---|---|
| Elements or oxides with content higher than their mean value throughout the region by 1.2 times | W, Cd | Au, As, Sb, Bi, Mo, B, Co, Cr, Cu, La, Ni, V, Y, Zn | Be, Sr, $Fe_2O_3$, $Na_2O$, CaO | F, Ti, Ba, Mn, Nb, P, CaO, MgO | Sr, V, $Fe_2O_3$, $Na_2O$, CaO | Ag, CaO | Au, Sb, Bi, Cd, B, Co, Cr, Cu, Ni, V, Y, Zn, $Fe_2O_3$ |
| Elements or oxides with content higher than their mean value and logarithmic variance throughout the region | Ag, Hg, Cd | Au, Ba, La, Nb | W, Be, Pb, $SiO_2$ | Mn | Sn | Cd | Au, Sb, Cu |

## 3.3    Element's Geochemistry Features

It was found from contents of elements in fluvial sediments of each geological sub−region that none of elements and oxides fit the normal distribution throughout the region, indicating that samples came from multiple parent bodies or that the region has undergone at least two geological or geochemical processes. Due to a heavier difference in geological background,

element content is not evenly distributed, resulting in a complicated probability distribution.

The mean contents of elements throughout the region and in each sub−region were counted to reflect variation characteristics of element content in different geological sub−regions (Table 3).

As shown in Table 3, Neogene sedimentary rock sub−region (N) is similar to Ordovician sedimentary rock sub-region (O) in combination of elements of which the contents in fluvial sediments are obviously higher than their background contents throughout the region, which are mainly precious metal Au, non−ferrous metals As, Sb, Bi, Mo, Cu, Zn, and siderophile elements Co, Cr, Ni, V and $Fe_2O_3$; three Neogene volcanic complex sub−regions (Nc, Np and Nv) enjoy combinations of elements and oxides with high contents such as Be, Sr, $Fe_2O_3$, $Na_2O$, CaO, MgO, Ti and V etc. In the Quaternary alluvium sub−region, W and Cd are abundant and in Paleogene sedimentary rock sub−region, Ag and CaO are enriched. High contents of these elements and oxides in fluvial sediments represent element geochemistry content distribution features in primary rocks in the region.

In the Ordovician sedimentary rock sub−region, Au, Sb and Cu in fluvial sediments are high in content and large in dispersion, indicating that the sub-region is an important metallogenic area for Au, Sb and Cu. In fact, vein−like Au, Sb−Au deposit and a small amount of hydrothermal breccia Sb-Au deposit exist in the Ordovician sedimentary rock.

## 4　Data Quality Control and Assessment

These 39 elements (oxides) were analyzed and tested by MNR's Changchun Mineral Resource Supervision and Testing Center. Elements and oxides analyzed are: B, Cd, As, Hg, Sb, Mo, F, Co, Cr, Cu, Mn, Ni, P, Pb, Zn, $SiO_2$, $Al_2O_3$, $Fe_2O_3$, $K_2O$, $Na_2O$, CaO, MgO, Ag, W, Sn, Bi, Au, Be, La, Nb, Li, Y, Zr, U, Th, V, Ti, Sr and Ba. They were analyzed mainly with X−ray fluorescence spectroscopy (XRF), combined with ICP−Ms (plasma-mass spectrometry), AFS (atomic fluorescence spectrometry), AES (atomic emission spectrometry), GFAAS (graphite furnace atomic absorption spectrometry) and ISE (ion selective electrode). Analysis methods, their detection limits, the detection limits specified in the regional geochemistry exploration specification (DZ/T0167-2006) and the reported percent for each element (oxide) are presented in Table 4.

**Table 4　Detection limits of analysis methods and the reported percent of analyzed elements**

| Element No. | Element detected | | Detection limit of analysis method | Detection limit specified in Specification | Reported percent (%) | Analysis method |
|---|---|---|---|---|---|---|
| 1 | As | Arsenic | 1 | 1 | 99.90 | AFS |
| 2 | B | Boron | 2 | 5 | 98.42 | AES |
| 3 | Sb | Antimony | 0.05 | 0.1 | 100.0 | AFS |
| 4 | Cd | Cadmium | 0.05 | 0.05 | 98.69 | ICP-Ms |
| 5 | Au | Gold | 0.3 | 0.3 | 99.95 | GFAAS |
| 6 | Co | Cobalt | 0.6 | 1 | 100.0 | ICP-Ms |
| 7 | Cr | Chromium | 5 | 15 | 100.0 | ICP-Ms |
| 8 | Cu | Copper | 1 | 1 | 100.0 | XRF |

Continued table 4

| Element No. | Element detected | | Detection limit of analysis method | Detection limit specified in Specification | Reported percent (%) | Analysis method |
|---|---|---|---|---|---|---|
| 9 | F | Fluorine | 100 | 100 | 100.0 | ISE |
| 10 | Hg | Mercury | 0.0005 | 0.0005 | 100.0 | AFS |
| 11 | Li | Lithium | 1 | 5 | 100.0 | ICP-Ms |
| 12 | Mn | Manganese | 13 | 30 | 100.0 | XRF |
| 13 | Mo | Molybdenum | 0.3 | 0.4 | 97.92 | ICP-Ms |
| 14 | Be | Beryllium | 0.4 | 0.5 | 100.0 | ICP-Ms |
| 15 | Ni | Nickel | 1.2 | 2 | 100.0 | ICP-Ms |
| 16 | P | Phosphor | 19 | 100 | 100.0 | XRF |
| 17 | Pb | Plumbum | 2 | 2 | 100.0 | XRF |
| 18 | U | Uranium | 0.3 | 0.5 | 100.0 | ICP-Ms |
| 19 | W | Tungsten | 0.3 | 0.5 | 99.97 | ICP-Ms |
| 20 | Zn | Zinc | 3 | 10 | 100.0 | XRF |
| 21 | Th | Thorium | 1 | 4 | 100.0 | ICP-Ms |
| 22 | Bi | Bismuth | 0.06 | 0.1 | 100.0 | ICP-Ms |
| 23 | $Al_2O_3$ | Aluminium oxide | 0.03 | 0.05 | 100.0 | XRF |
| 24 | $SiO_2$ | Silicon dioxide | 0.06 | 0.1 | 100.0 | XRF |
| 25 | $Fe_2O_3$ | Iron sesquioxide | 0.04 | 0.05 | 100.0 | XRF |
| 26 | CaO | Calcium oxide | 0.02 | 0.05 | 100.0 | XRF |
| 27 | MgO | Magnesium oxide | 0.04 | 0.05 | 100.0 | XRF |
| 28 | $K_2O$ | Potassium oxide | 0.02 | 0.05 | 100.0 | XRF |
| 29 | $Na_2O$ | Sodium oxide | 0.03 | 0.05 | 100.0 | XRF |
| 30 | Nb | Niobium | 1 | 5 | 100.0 | XRF |
| 31 | Sr | Strontium | 3 | 5 | 100.0 | XRF |
| 32 | Ti | Titanium | 30 | 100 | 100.0 | XRF |
| 33 | V | Vanadium | 4 | 20 | 100.0 | ICP-Ms |
| 34 | Y | Yttrium | 1 | 5 | 100.0 | XRF |
| 35 | Zr | Zirconium | 2 | 10 | 100.0 | XRF |
| 36 | Ba | Barium | 13 | 50 | 100.0 | XRF |
| 37 | La | Lanthanum | 8 | 30 | 100.0 | XRF |
| | La | Lanthanum | 1 | 30 | 100.0 | ICP-Ms |
| 38 | Sn | Tin | 0.8 | 1 | 100.0 | AES |
| 39 | Ag | Silver | 0.02 | 0.02 | 99.97 | AES |
| Total | | | | | 99.86 | |

Note: XRF, X−ray fluorescence spectroscopy; ICP−Ms, plasma-mass spectrometry; AFS, atomic fluorescence spectrometry; AES, atomic emission spectrometry; GFAAS, graphite furnace atomic absorption spectrometry; and ISE, ion selective electrode.

Internal and external quality controls were combined, with the external quality control being the focus for quality management. For external quality control, 208 standard control samples were interpolated as per the percentage of 8%. For internal quality control, 4 level-1 standard materials (GSD2a, GSD8a, GSD22 and GSD4a) for fluvial sediments were interpolated into each group of 50 analytic samples to calculate the logarithmic difference between each measurement and standard value in order to control analytical accuracy; the standard deviation of the logarithmic difference of 4 control samples were calculated to assess the precision of the same lot of samples.

Quality control of Au analysis: 4 standard materials (GAu2b, GAu7b, GAu10b and GAu11b, with contents of 0.9, 3.1, 5.1 and 10.5 respectively), as Au analysis control sample, were interpolated into every 50 samples.

Quality control of internal−inspection samples and anomaly points: 5% of the total samples were taken as an internal−inspection sample for inspection and analysis. Samples with higher or lower contents of elements were randomly inspected for their anomaly values. For quality control of internal inspection and anomaly−value random inspection of elements (or items), the qualified rate was calculated as per $|RD\%|\leqslant 25\%$.

The qualified rates of all control samples for 39 elements were 100%.

These 132 samples for internal inspection were randomly taken, accounting for 5% of the total samples delivered constituting 5,148 items for internal inspection, and the overall qualified rate of internal inspection was 99.51%.

To avoid any misleading conclusions due to accidental error from the analysis, high and low saltation points of some analytical results were inspected repeatedly after analyzing each lot of samples. In total, 1,153 items were randomly inspected for anomaly points, of which 1,142 items were acceptable, and the overall qualified rate was 99.04%. The overall qualified rate of internal-inspection samples and anomaly−value random inspection together was 99.42%.

## 5  Data Processing

The data processing software Geoexpl 2012, developed by the Development and Research Center of China Geological Survey, was used in data processing and map plotting. Method for Data Processing:

(1) Data gridding

The grid spacing was 4 km×4 km, the search radius was 10 km, and the index weighting method was used.

(2) Element's geochemical map

A computer was used to directly plot the isogram map using grid data with an area of 4 $km^2$. The accumulative frequency diversity method was used to determine the interval between isograms. For color zones, the accumulative frequency method was used to plot the maps, and color zones were divided into deep blue (<1.5%), blue (1.5%~15%), shallow blue (15%~25%), light yellow (25%~75%), light red (75%~85%), deep red (95%~98.5%) and deep red (>98.5%).

(4) Quality Assurance

During the plotting of the map, information collation, transcription and calculation, all raw data was rechecked 100%.

## 6 Conclusions

For 4 years, the Argentine Mina Pirquitas 1 ∶ 250 000 fluvial sediment geochemical map plotting was done jointly by CGS and AGS. The precious first−hand geochemistry data and information were obtained, including raw analytical data on 39 elements and oxides from 2 470 fluvial sediment and soil samples, and a series of geochemical maps plotted on this basis. The 487 locations exhibiting single−element geochemistry anomaly and 52 locations with comprehensive anomaly were newly discovered, along with the delineation of two prospective areas worth further investigation. Further research and mining information from these data and maps are important for reference to mineral exploration, fundamental geological research and environmental engineering in the region.

## References

Bahiburg H., Breitkreuz C. 1991. Paleozoic Evolution of Active Margin Basins in the Southern Central Andes (Northwestern Argentina and Northern Chile)[J]. Journal of South American Earth Sciences, 4(3): 171−188.

Chen Nian, Mao Jingwen, Fan Chenglong, Chen Yuming. 2017. Alteration-mineralization characteristics and three-dimensional exploration model of Don Javier porphyry copper-molybdenum deposit, Peru[J]. Mineral Deposits, 36(3): 705−718 (in Chinese with English abstract).

Chen Xifeng, Ye Jinhua, Xiang Yunchuan. 2017. On Development Situation and Bauxite Potentiatity of South Americas Resources[J]. Scientific and Technological Management of Land and Resources, 34(1): 106−115 (in Chinese with English abstract).

Chen Yuming, Deng Xiaolin. 2013. The Lithium Resources Potential and Utilization in Argentina[J]. Journal of Salt Lake Research, (4): 67−72 (in Chinese with English abstract).

Chen Yuming, Xia Xiuzhan, Gan Qiuling, Geng Lin, Yang Gang. 2016. Test study on particle size sampling of stream sediment in Minas Pirquitas Area of Argentina[J]. Contributions to Geology and Mineral Resources Research, 31(2): 295−302 (in Chinese with English abstract).

Chen Yuming, Zhang Chao, Chen Xiufa. 2017. Geological Minerals and Mining Development of South America[M]. Wuhan: China University of Geosciences Press (in Chinese).

Cui Minli, Zhang Zuolun, Chen Yuming, Chen Fangge. 2017. Geology and metallogenic process of large and super—large gold deposits inSouth America[J]. Geology in China, 44(4): 642−663 (in Chinese with English abstract).

Flexer Victoria, Fernando Baspineiro Celso, Ines Galli, Claudia. 2018. Lithium Recovery from Brines: A Vital Raw Material for Green Energies with a Potential Environmental Impact in Its Mining and

Processing[J]. Science of the Total Environment, 639: 1188−1204.

Rafaerl A. A. 1999. Depositos de Sulfato de Sodio de Jujuy, Salta y Catamarca[M]. Eduardo O. Zappettini, Recursos Minerale de la Republica Argentian, Publicado con la Colaboracion de la Fundacion Empremin, Buenos Aires, Instituto de Geologia y Minerales−SEGEMAR, 1922−1925.

Ricardo N. Alonso, 1999a. Boratos terciarios de la Puna, Jujuy, Salta y Catamarca [M]. Eduardo O. Zappettini, Recursos Minerale de la Republica Argentian, Publicado con la colaboracion de la Fundacion Empremin, Buenos Aires, Instituto de Geologia y Minerales−SEGEMAR: 1779−1826.

Ricardo N. Alonso. 1999b. Los Salares de la Puna y sus Recursos Evaporiticos, Jujuy, Salta y Catamarca [A]. Eduardo O. Zappettini, Recursos Minerale de la Republica Argentian[C]. Publicado con la colaboracion de la Fundacion Empremin, Buenos Aires, Instituto de Geologia y Minerales−SEGEMAR: 1905−1921.

Voldman Gustavo G., Alonso Juan L., Fernandez Luis P 2018. Cambrian-Ordovician Conodonts from Slump Deposits of the Argentine Precordillera: New Insights into Its Passive Margin Development[J]. Geological Magazine, 155(1): 85−97.

Zhang Chao, Chen Yuming, Zhao Hongjun, Yao Zhongyou, Guo Weiming. 2017. Division of metallogenic units and geological characteristics in South America[J]. Geological Bulletin of China, 36(12): 2134−2142 (in Chinese with English abstract).

Zhang Chao, Chen Yuming, Chen Xifeng, Yao Zhongyou, Guo Weiming. 2017. Spatial-temporal distribution regularity of gold deposits in Argentina[J]. Geological Bulletin of China, 36(12): 2154−2163 (in Chinese with English abstract).

Zhang Chao, Chen Yuming, Zhao Hongjun, Yuan Chunhua. 2017. Spatial-Temporal Distribution Regularity of the Copper Deposits in South America[J]. Geological Review, 63(S1): 29−30 (in Chinese with English abstract).

Zhang Chao, Chen Yuming, Zhao Hongjun. 2017. The Tectono-magmatic Events and Mineralization in the Central Andes of South America[J]. Geological Review, 63(S1.): 17−18(in Chinese).